RSC Advances

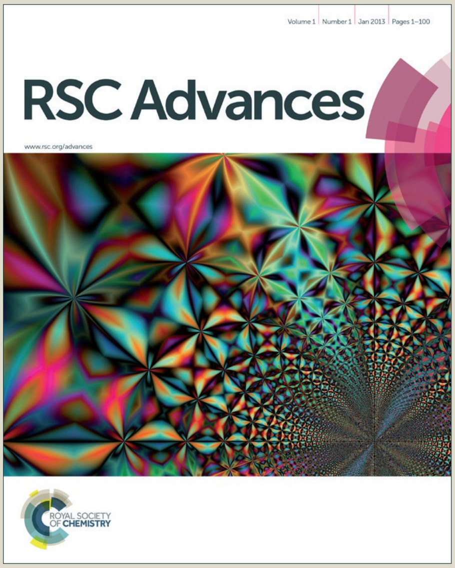

ROYAL SOCIETY OF CHEMISTRY

www.rsc.org/advances

Improved electrochemical properties of $LiMn_2O_4$ with the Bi and La co-doping for lithium-ion batteries

Cheng-Gong Han, Chunyu Zhu, Genki Saito, Tomohiro Akiyama[*]

Center for Advanced Research of Energy and Materials, Hokkaido University, Sapporo 062-8628, Japan

Abstract: A series of $LiBi_xLa_xMn_{2-2x}O_4$ (x=0, 0.002, 0.005, 0.010, 0.020) samples were synthesized by solution combustion synthesis in combination with calcination. The phase structure and morphology of the products were characterized by X-ray diffraction, scanning electron microscopy, and transition electron microscopy. The results demonstrated that a single-phase $LiMn_2O_4$ spinel structure was obtained for the $LiBi_xLa_xMn_{2-2x}O_4$ (x=0, 0.002, 0.005) samples, whereas impurities were observed for the $LiBi_xLa_xMn_{2-2x}O_4$ (x=0.010, 0.020) samples as a result of the doping limit. The electrochemical properties were investigated by galvanostatic charge–discharge cycling and cycling voltammetry in a voltage range of 3.2–4.4 V. The substitution of Mn^{3+} by equimolar Bi^{3+} and La^{3+} could significantly improve the structural stability and suppress the Jahn–Teller distortion, thereby resulting in improved electrochemical properties for the Bi and La co-doped samples in contrast with the pristine $LiMn_2O_4$ sample. In particular, the $LiBi_{0.005}La_{0.005}Mn_{1.99}O_4$ sample delivered a high initial discharge capacity of 130.2 mAh/g at 1 C, and following 80 cycles, the capacity retention was as high as 95.0%. Moreover, it also presented the best rate capability among all the samples, in which a high discharge capacity of 98.3 mAh/g was still maintained at a high rate of 7 C compared with that of 75.8 mAh/g for the pristine $LiMn_2O_4$ sample.

Keywords: $LiMn_2O_4$, Cathode material, Bi and La doping, Li-ion batteries

---

[*] Corresponding author. Tel.: +81 11 706 6842; fax: +81 11 726 0731.
E-mail address: takiyama@eng.hokudai.ac.jp (T. Akiyama)

1. Introduction

Rechargeable Li-ion batteries are considered to be the most promising energy-storage devices for powering electric vehicles (EVs) and hybrid EVs because of their high volumetric/gravimetric energy density, and long cycling life.[1-5] The low cost, high safety, high capacity, and good rate capability of Li-ion batteries adapted for further commercialized applications are closely linked to the cathode, anode, and electrolyte materials used, especially cathode materials because they exhibit a much lower capacity than anode materials.[6] Amongst many cathode materials, $LiMn_2O_4$ has been particularly highlighted as an appropriate and attractive cathode because of its low cost, high safety, environmental friendliness, and good electrochemical performance at high currents.[7,8] Spinel $LiMn_2O_4$ material has a cubic structure with the space group of *Fd3m*, in which Mn ions occupy the 16d octahedral sites while Li ions are located at the 8a tetrahedral sites and quickly diffuse through cross-linked 1×3 channels formed by the edge-shared MnO_6 frame. This supports good electrochemical performance even at high current rates.[7] However, in the 4 V region, $LiMn_2O_4$ cathode materials undergo severe capacity fading during repeated cycling. This mainly results from (1) Jahn–Teller distortion inducing the irreversible phase transition from the cubic phase to tetrahedral phase; and (2) the dissolution of Mn^{2+} into the electrolyte solution resulting from the disproportional reaction, $2Mn^{3+} \rightarrow Mn^{2+} + Mn^{4+}$. [9,10]

Up to now, two main strategies, surface modification[11,12] and doping technology[13,14], have been developed to solve the aforementioned capacity fading issue. Surface modification can decrease the contact areas between the $LiMn_2O_4$ particles and the electrolyte solution, and therefore inhibit the manganese dissolution. However, surface modification technology usually impairs the capacity and scarcely alleviates the Jahn–Teller distortion.[15] Recently, the doping of one or more elements at the manganese sites has been proposed as an effective method to alleviate capacity fading by reducing the Jahn–Teller distortion and the dissolution of manganese in the electrolyte solution.[14,16] The single element doping of $LiMn_2O_4$ has been widely performed using a small amount of trivalent ions, such as Co^{3+},[17] Al^{3+},[18,19] Fe^{3+},[20] Cr^{3+},[21] Ga^{3+},[22,23] Sm^{3+},[24,25] La^{3+},[26,27] resulting in an improved cycling performance during the charge/discharge process. By contrast, $LiMn_2O_4$ with the substitution of multiple ions has received more attention because of the occurrence of the synergistic effect, which improves the cycling life.[28-31] Mohan et al. demonstrated that La and Sm co-substituted $LiSm_xLa_{0.2-x}Mn_{1.80}O_4$ (x=0.05, 0.10, 0.15) cathode materials synthesized by the sol-gel method exhibited enhanced structural stability of the octahedral sites in the spinel structure with the substitution of a small amount of La and Sm. This resulted in improved capacity retentions of 90% and 82% for the $LiSm_{0.10}La_{0.10}Mn_{1.80}O_4$ sample, compared with those of 74% and 60% for the pristine $LiMn_2O_4$ after 100 cycles at a current density of 0.5 C at temperatures of 30 °C and 50 °C, respectively.[32] Iqbal et al. prepared La and Zn co-doped $LiMn_2O_4$ spinel materials using a sol-gel method.[33] The results revealed that the $LiLa_{0.01}Zn_{0.01}Mn_{1.98}O_4$ sample achieved a higher discharge capacity of 92 mAh/g and 78% of the initial discharge capacity at 5 C compared to values of 51 mAh/g and 41% for the un-doped $LiMn_2O_4$ sample. This indicates that the La and Zn co-doping stabilized the structural integrity of the spinel host by suppressing the Jahn–Teller distortion and shortening the diffusion of the Li ions. La, a rare earth metal, can be selected as a possible candidate to function as a substitute for manganese because of its large binding energy, therefore forming a pillar and preventing the collapse of the cubic structure, and increasing the average valence of Mn, thereby reducing the occurrence of the Jahn–Teller distortion.[26,33,34] Moreover, the heavy element, bismuth, has been found to partially substitute manganese as a dopant.[35,36] From electrochemical investigations in a strong alkaline electrolyte (9M KOH), Schlörb et al. reported that Bi-doped $LiMn_2O_4$ material achieved remarkably improved cyclability, whereas after 10 cycles, a rapid decrease in capacity to 50% of the initial value was observed for the un-doped $LiMn_2O_4$ sample.[36] Following 100 cycles measured at a constant current of 40 mA/g, Tan et al. demonstrated that Bi-modified $LiMn_2O_4$, synthesized by a sol-gel method, achieved a discharge capacity of 100 mAh/g and a capacity retention of 84.7%, compared with a capacity retention of 74.2% for the unmodified sample.[37] When the heavy element, bismuth, is introduced to the spinel structure, it can result in the hybridizing of the 6s and 6p orbitals of the bismuth ions with the adjacent 2p orbital of the oxygen in addition to the 3d orbital of the manganese.[38] Doped bismuth ions can increase the charge transfer from the oxygen anion to the manganese cation because of the overlapping of the bismuth orbital with the oxygen and manganese orbitals. This probably results in a wider conduction band, increasing the electronic conductivity and lithium diffusivity of the electrodes.[38,39] Considering the lack of studies on Bi and La co-doping, Bi and La are introduced to partially substitute Mn in order to improve both the stability of the spinel structure and the electrochemical performance during this study.

In this work, a novel solution combustion synthesis (SCS) method was employed because it can be used to homogeneously dope elements in trace amounts and yield nano-sized particles with high specific areas, thus benefitting the electrochemical properties.[40] Bi and La were selected as the doping elements to partially substitute Mn in order to improve the electrochemical properties of the $LiMn_2O_4$ material. Considering the above, $LiBi_xLa_xMn_{2-2x}O_4$ (x=0, 0.002, 0.005, 0.010, 0.020) samples were synthesized by the SCS method in combination with calcination. The effect of the Bi and La doping amounts on the structure, morphology, and electrochemical performance was investigated in detail.

2. Experimental

2.1 Preparation and characterization of Bi and La co-doped $LiMn_2O_4$ cathode materials.

Bi and La co-doped $LiMn_2O_4$ samples were prepared by solution combustion synthesis (SCS) in combination with calcination. Stoichiometric amounts of oxidizers, lithium nitrate ($LiNO_3$, 99.0%, Kishida Chemical Co., Ltd., Japan), bismuth nitrate ($Bi(NO_3)_3{\cdot}5H_2O$, 99.5%, Kanto Chemical Co., Inc., Japan), lanthanum nitrate ($La(NO_3)_3{\cdot}6H_2O$, 99.9%, Wako Pure Chemical Industries, Ltd., Japan), and manganese nitrate ($Mn(NO_3)_2$, 50% w/w aqueous solution, Alfa Aesar) were dissolved in 5 ml of distilled water in terms of $LiBi_xLa_xMn_{2-2x}O_4$ (x=0, 0.002, 0.005, 0.010, 0.020). A corresponding amount of urea (NH_2CONH_2, 99.0%, Chameleon Reagent, Japan) as the reductant (with φ=0.5, φ is the ratio of the total valence of reductants to the total valence of nitrate oxidizers) was also added into the above solutions. The homogenous sol-gels were formed by evaporating the water at 350 rpm at a temperature of 90 °C. The obtained sol-gels self-ignited in a homemade combustion synthesis apparatus, which was placed into a constant temperature laboratory electric jacket that was pre-heated and maintained at a temperature of 400 °C. The power of the electric jacket was switched off once the combustion reaction associated with the gas emission was observed. Following the SCS, the collected powders were further calcined at 800 °C for 24 h at a rate of 5 °C/min in air to obtain the final powders.

The phase structure was characterized by powder X-ray diffraction (XRD, Cu Kα, Rigaku Miniflex). The morphology, size of the powders, the energy-dispersive spectroscopy (EDS), the electron energy-loss spectroscopy (EELS), and the energy dispersive X-ray spectroscopy (EDX) were determined by scanning electron microscopy (SEM, JEOL, JSM-7001FA) and transmission electron microscopy (TEM, JEOL JEM-2010F).

2.2 Cell assembly and electrochemical measurement.

A two-electrode Swagelock-type cell consisting of a working electrode and a lithium metal anode was employed. It was assembled in an Ar-filled glove box, as described in our previous reports.[40,41] The working electrode contained 80 wt.% active materials, 10 wt.% polymer binder (polyvinylidene fluoride (PVDF)) dissolved in an N-methyl-2-pyrrolidone (NMP) solution, and 10 wt.% conductive carbon (acetylene black). The above mixture was magnetically stirred to form a homogenous slurry. The slurry was cast on an aluminum foil current collector and subsequently dried in a vacuum oven at 110 °C over a period of 12 h. The dried aluminum foil electrode was punched into disks with a diameter of 10 mm and a thickness of 0.1 mm. Meanwhile, a lithium metal disk with a diameter of 10 mm was selected as the counter and reference electrode. A solution of 1 M lithium hexafluorophosphate ($LiPF_6$) in ethylene carbonate (EC)/dimethyl carbonate (DMC) (1:1 in volume) was used as the electrolyte while a celgard polypropylene membrane was employed as the separator. The electrochemical measurements were performed galvanostatically within the voltage range of 3.2–4.4 V with a current density of 1 C (a rate of 1 C corresponds to a full charge/discharge of 150 mAh/g in 1 h) at the temperature of 25 °C using a battery tester (Arbin Instrument, MSTAT4, USA). Cyclic voltammetry (CV) was performed using the potentiostat/glavanostat apparatus (Autolab, PGSTAT128N).

3. Results and discussion

Fig. 1 shows the XRD patterns of the $LiBi_xLa_xMn_{2-2x}O_4$ (x=0, 0.002, 0.005, 0.010, 0.020) samples, with the enlarged (111) diffraction peak on the left. All the diffraction peaks of the $LiBi_xLa_xMn_{2-2x}O_4$ (x=0, 0.002, 0.005) sample well correlate with the standard peaks of the spinel-structure, indicating the successful synthesis of the single-phase $LiMn_2O_4$ by the SCS in combination with calcination. However, only the main diffraction peaks can be indexed to the $LiMn_2O_4$ phase for the $LiBi_xLa_xMn_{2-2x}O_4$ (x=0.010, 0.020) samples. The $LaMnO_{3.15}$ impurity phase can be detected in the $LiBi_{0.01}La_{0.01}Mn_{1.98}O_4$ and $LiBi_{0.02}La_{0.02}Mn_{1.96}O_4$ samples while an extra Bi_2O_3 impurity phase can be observed in the $LiBi_{0.02}La_{0.02}Mn_{1.96}O_4$ sample because of the doping limit. The shift to a lower angle for all diffraction peaks, especially the (111) peak as the most intense peak, is observed after the co-doping of Bi and La based on the character of the cubic structure. The 2θ angle of the (111) diffraction peak shifts to a lower angle as the x values increase, indicating the enlargement of the lattice parameters for the Bi and La co-doped $LiMn_2O_4$ samples. And the explanation will be shown in the following Fig. 2.

Fig. 2 displays the lattice parameters of the $LiBi_xLa_xMn_{2-2x}O_4$ (x=0, 0.002, 0.005, 0.010, 0.020) samples. All the lattice parameters are refined by MDI Jade Software. The enlarged lattice parameters of the $LiBi_xLa_xMn_{2-2x}O_4$ samples can be observed as x increases from 0 to 0.01, indicating that Mn^{3+} with a smaller ionic radius, 0.72 Å, is substituted by Bi^{3+} and La^{3+} with the same ionic radius, 1.03 Å. However, as x increases from 0.01 to 0.02, the lattice parameters of the Bi and La co-doped samples are relatively constant, demonstrating that the amount of Bi and La doping attains a limit which results in the $LaMnO_{3.15}$ and Bi_2O_3 impurities shown in Fig. 1. The enlargement of the lattice parameters indicates that Bi and La enter the spinel structure, probably benefiting the improved electrochemical properties of the $LiMn_2O_4$ materials as a result of the enlarged Li^+ diffusion channel during the intercalation/de-intercalation process.

Fig. 3 shows the SEM images of the $LiBi_xLa_xMn_{2-2x}O_4$ (x=0, 0.002, 0.005, 0.010, 0.020) samples. All the samples exhibit similar morphologies. There are no obvious changes in the morphologies or particle sizes of the Bi and La co-doped samples, indicating that the trace doping of Bi and La does not have a significant effect on the morphologies or particle sizes of the co-doped samples. The size of the primary particles in the inset is 100–400 nm. Asymmetrical spheres with a size of 3–7 μm can be observed in the secondary particles.

Fig. 4 demonstrates the discharge capacity as a function of the cycle number at a current density of 1 C in the voltage range of 3.2–4.4 V for the $LiBi_xLa_xMn_{2-2x}O_4$ (x=0, 0.002, 0.005, 0.010, 0.020) samples. The pristine $LiMn_2O_4$ sample exhibits an initial discharge capacity of 121.3 mAh/g and only maintains a capacity retention of 89.0% after 80 cycles. As the x value is increased from 0 to 0.002 and 0.005, the initial discharge capacity of the Bi and La co-doped $LiMn_2O_4$ sample improves, exhibiting values of 128.7 and 130.2 mAh/g for x=0.002 and 0.005, respectively. A remarkably improved capacity retention of 95.0% and a discharge capacity of 123.7 mAh/g are delivered for the $LiBi_{0.005}La_{0.005}Mn_2O_4$ sample after 80 cycles, indicating that a more stable structure is achieved during the Li-ion intercalation/de-intercalation process compared with the pristine $LiMn_2O_4$. Both this capacity retention and discharge capacity are higher than the values of 89.1% and 106 mAh/g after 50 cycles at the current density of 1 C for the $LiLa_{0.05}Mn_{1.95}O_4$ sample by the sol-gel method,[26] and the values of 91.6% and 103.7 mAh/g after 100 cycles at the current density of 0.2 C for the $LiLa_{0.05}Mn_{1.95}O_4$ sample by the solid state reaction.[27] In addition, these values are also higher than that of 84.7% and 100 mAh/g after 100 cycles at the current density of near 0.3 C for the Bi-modified $LiMn_2O_4$ sample which a trace doping amount of Bi is verified by the increased lattice parameters calculated from XRD results.[37] The detailed dates of the current and reported works are also shown in the Table 1. This result indicates that co-doping is superior to single-doping for improving the electrochemical properties of $LiMn_2O_4$ material because of their synergistic effects. These results can be attributed to the factors discussed below. The bond energy of La-O (786.2 KJ/mol) for the doped sample is greater than that of Mn-O (402 KJ/mol), which can improve the spinel structure during cycling. What's more, both the dissolution of Mn^{3+} into the electrolyte and the Jahn–Teller distortion are inhibited because the relatively partial amount of Mn^{3+} is reduced by the substitution of Bi^{3+} and La^{3+}, as demonstrated in Fig. 7 (d). Moreover, the diffusion of the Li ions for the insertion/extraction is enhanced probably owing to the amplified channels resulting from the enlarged lattice parameters of the Bi and La co-doped $LiMn_2O_4$ sample.[15,32,39] On the other hand, the improved cycling performance of the $LiBi_{0.005}La_{0.005}Mn_{1.99}O_4$ sample can also be confirmed by the less capacity fade of 0.08 mAh/g cycle^{-1} than that of 0.19 mAh/g cycle^{-1} for the pristine $LiMn_2O_4$ sample, displaying that the substitution of Mn by the partial amounts of Bi and La is in favor of enhancing the cycling performance. The discharge capacity of the Bi and La co-doped $LiMn_2O_4$ with x values of 0.010 and 0.020 is less than that of the $LiBi_{0.005}La_{0.005}Mn_2O_4$ sample which can be attributed to the appearance of the second phase. However, following the 80 cycles, a slightly improved capacity retention of 90.8% is achieved for the $LiBi_{0.02}La_{0.02}Mn_2O_4$ sample compared with that of the pristine $LiMn_2O_4$, which may be ascribed to the coating effect of the Bi_2O_3 second phase on the surface of the particles.[24] The appropriate amounts of Bi and La doping can improve the cycling performance of the spinel $LiMn_2O_4$ material.

The charge–discharge curves of the $LiBi_xLa_xMn_{2-2x}O_4$ (x=0, 0.002, 0.005, 0.010, 0.020) samples for the 1st and 80th cycles are shown in Fig. 5 (a) and (b), respectively, at a current density of 1 C between voltages of 3.2 and 4.4 V. Two obvious plateaus can be observed in the voltage range of 3.9 to 4.2 V for all the charge–discharge curves, which can be attributed to the well-defined spinel structure of $LiMn_2O_4$.[32] These two plateaus correspond to two oxidation/reduction reaction stages during the Li de-insertion/insertion process. The first plateau at approximately 4.0 V results from the removal of Li^+ ions from half of the tetrahedral sites in which Li–Li interactions occur. The second plateau at approximately 4.1 V can be attributed to the removal of Li^+ ions from the other tetrahedral sites. Among these samples, the $LiBi_{0.005}La_{0.005}Mn_{1.99}O_4$ sample exhibits the highest discharge capacity for both the 1st and 80th cycles.

Fig. 6 presents the CV curves of the $LiBi_xLa_xMn_{2-2x}O_4$ (x=0, 0.005) samples in the voltage range of 3.2–4.4 V at a scan rate of 0.1 mV/s. For comparison, the CV was only conducted for the pristine $LiMn_2O_4$ and $LiBi_{0.005}La_{0.005}Mn_{1.99}O_4$ samples. Two pairs of clearly separated redox peaks were observed in the CV curves of the pristine $LiMn_2O_4$ and $LiBi_{0.005}La_{0.005}Mn_{1.99}O_4$ samples. These can be ascribed to two typical reversible processes during the Li^+ intercalation/de-intercalation cycling which correspond to the two plateaus in the charge–discharge curves of Fig. 5. The peak parameters of the CV curves during the first cycle of the pristine $LiMn_2O_4$ and $LiBi_{0.005}La_{0.005}Mn_{1.99}O_4$ samples are listed in Table 2. A cathodic peak of 3.94/4.06 V and anodic peaks of 4.07/4.20 V can be observed for the pristine $LiMn_2O_4$ sample while a cathodic peak of 3.96/4.08 V and anodic peaks of 4.05/4.18 V can be observed for the $LiBi_{0.005}La_{0.005}Mn_{1.99}O_4$ sample. The anodic peaks shift to a lower potential for the doped $LiMn_2O_4$ sample compared with the pristine $LiMn_2O_4$ sample, indicating that a portion of Li^+ ions can migrate under less energy from the distorted spinel structure of Mn^{3+} substituted by Bi^{3+} and La^{3+}.[32,42] A larger cathodic potential difference, ΔE_1=0.13 V, and anodic potential difference, ΔE_2=0.14 V, are exhibited for the pristine $LiMn_2O_4$ sample. However, clearly reduced values of ΔE_1=0.09 V and ΔE_2=0.10 V are observed for the $LiBi_{0.005}La_{0.005}Mn_{1.99}O_4$ sample. This suggests that there is a reduced polarization of the Bi and La co-doped $LiMn_2O_4$ material owing to faster intercalation/de-intercalation of Li^+ ions into/from the spinel structure compared with the pristine sample.[24,33,43] The substitution of Mn^{3+} with Bi^{3+} and La^{3+} cations can maintain the stability of the spinel structure, therefore improving the cycling performance of the materials during the charge/discharge process.

Fig. 7 (a) and (b) display the TEM image with the electron diffraction pattern of the [110] zone axis within the inset, and the EDX analysis for the $LiBi_{0.005}La_{0.005}Mn_{1.99}O_4$ sample, respectively. The TEM image shows primary particles with a size of approximately 300 nm, which corresponds to the SEM image in Fig. 3. As there is no evidence of the surface coating layer exhibited in either the morphology shown in the TEM image or the single phase indexed from the XRD patterns in Fig. 1, it can be confirmed that the co-doped Bi and La ions enter into the structure of the $LiBi_{0.005}La_{0.005}Mn_{1.99}O_4$ sample. The electron diffraction pattern demonstrated in the inset exhibits typical spinel structure diffraction along the [110] direction, correlating with Fig. 1. To analyze the change in the valence states before/after the La and Bi doping, the EELS data was measured for the obtained particles. Fig. 7 (c) and (d) show the oxygen (O) K-edge and manganese (Mn) L-edge EELS of the $LiBi_xLa_xMn_{2-2x}O_4$ material with $x = 0$ and 0.005, respectively. The spectra positions can be calibrated from their zero-loss peaks. The peaks of Mn–L_3 and Mn–L_2 result from the transition of electrons from $2p_{3/2}$ to $3d_{3/2}$ and $3d_{5/2}$, and from $2p_{1/2}$ to $3d_{3/2}$, respectively.[44] These relative intensities can be determined by the unoccupied bands in the 3d orbitals and therefore the valence state of Mn.[45] The L_3/L_2 intensity ratio is related to the valence state of Mn.[46,47] Compared with Fig. 7 (c) and (d), following the Bi and La co-doping there is a decrease in the L_3/L_2 intensity ratio which indicates an increase in the Mn oxidation state. Specifically, following the Bi and La co-doping, a relatively greater amount of Mn^{4+} appear, arising from the substitution of Bi^{3+} and La^{3+} at the Mn^{3+} sites. In order to identify the existence and distribution of the Bi and La, the EDS of the $LiBi_{0.005}La_{0.005}Mn_{1.99}O_4$ sample is shown in Fig. 8. The peaks relating to Bi and La confirm the existence of these two elements while the element maps demonstrate the uniform distribution of the Bi and La in the $LiBi_{0.005}La_{0.005}Mn_{1.99}O_4$ sample.

Good rate capability, especially the discharge capacity at high current densities, is always required for high power applications of Li-ion batteries. Fig. 9 shows the rate capability of the $LiBi_xLa_xMn_{2-2x}O_4$ (x=0, 0.002, 0.005, 0.010, 0.020) samples in the voltage range of 3.2–4.3 V. All the samples exhibit decreased capacities as the current densities are increased, which can be attributed to the increased ohmic and electrochemical polarization arising from the limited diffusion of the Li^+ ions into/out of the spinel structure.[15,48] The pristine $LiMn_2O_4$ sample exhibits an initial discharge capacity of 120.3 mAh/g at a current density of 1 C and a dramatically decreased value of 75.8 mAh/g at a high current of 7 C. However, among all the samples, the best rate capability was achieved in the $LiBi_{0.005}La_{0.005}Mn_{1.99}O_4$ sample, exhibiting discharge capacities of 127.6 (1 C), 120.8 (2 C), 115.1 (3 C), 111.0 (4 C), and 106.8 mAh/g (5 C). The high value of 98.3 mAh/g is still maintained even at a high current of 7 C. The superior rate capability can be attributed to the broadened diffusion pathway of the Li^+ ions during the intercalation/de-intercalation as a result of the enlarged lattice parameters and improved stable structure via the substitution of Mn^{3+} with a suitable amount of Bi^{3+} and La^{3+} cations.[15,32,39]

Fig. 10 shows the discharge curves for the $LiBi_{0.005}La_{0.005}Mn_{1.99}O_4$ sample at various current densities. Two obvious plateaus can be observed in the discharge curve at 1 C, 2 C, and 3 C; however, the plateaus gradually disappear to transform into the slope at a high current density, such as 7 C. This can be attributed to the ohmic drop and the increase in the cell polarization at high current densities.[5] The discharge capacity as a function of the cycle number at current densities of 1 C, 3 C, and 5 C between the voltage of 3.2 and 4.4 V is presented in Fig. 11 for the $LiBi_{0.005}La_{0.005}Mn_{1.99}O_4$ sample. The $LiBi_{0.005}La_{0.005}Mn_{1.99}O_4$ sample exhibits good capacity retention at current densities of 3 C and 5 C. Even after 500 cycles, it delivers a discharge capacity of 105.9 mAh/g at 3 C and 101.1 mAh/g at 5 C, exhibiting the best high-rate capability.

4. Conclusions

A single-phase spinel structure was synthesized for the $LiBi_xLa_xMn_{2-2x}O_4$ (x=0, 0.002, 0.005) samples via SCS followed by calcination, while impurities were detected in the x=0.010, 0.020 samples because of the doping to an extent. As the x values were increased, the increase in the lattice parameters indicated that Bi and La entered the spinel structure. Following 80 cycles, the $LiBi_{0.005}La_{0.005}Mn_{1.99}O_4$ sample delivered the highest initial discharge capacity of 130.2 mAh/g and 95% capacity retention at 1 C compared with values of 121.3 mAh/g and 89% for the pristine $LiMn_2O_4$ sample. Even after 500 cycles, high capacities of 105.9 mAh/g at 3 C and 101.1 mAh/g at 5 C were still maintained for the $LiBi_{0.005}La_{0.005}Mn_{1.99}O_4$ sample, thus achieving the best high-rate capability. The improved electrochemical properties of the Bi and La co-doped $LiMn_2O_4$ material can be attributed to the good stability of the spinel structure and the high level of diffusion of the Li ions in/out the enlarged structure.

Acknowledgement

We would like to thank "Nanotechnology Platform" Program of the Ministry of Education for allowing us to use transmission electron microscope observation, the partially financial support by the Japan Society for Promotion of Science (JSPS) and Japan Science and Technology Agency (JST).

Figures

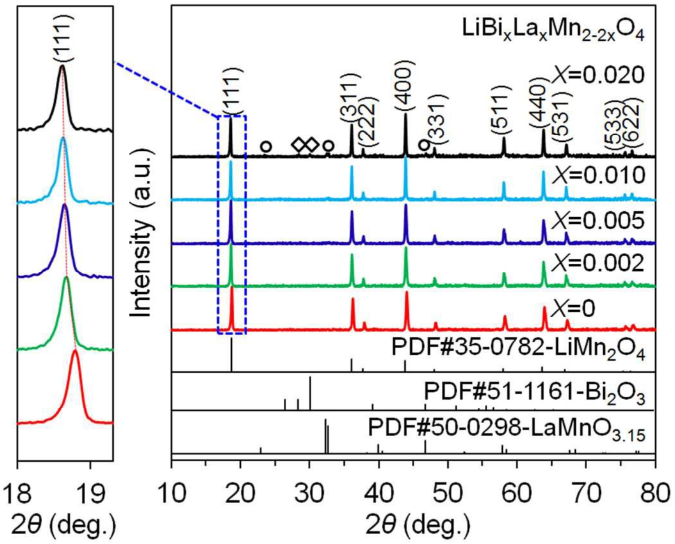

Fig. 1 XRD patterns of LiBi$_x$La$_x$Mn$_{2-2x}$O$_4$ (x=0, 0.002, 0.005, 0.010, 0.020) samples with the enlarged (111) diffraction peak.

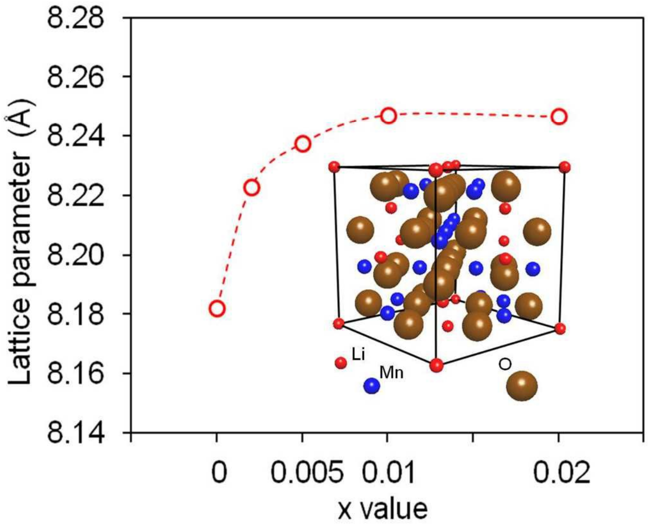

Fig. 2 Lattice parameters of LiBi$_x$La$_x$Mn$_{2-2x}$O$_4$ (x=0, 0.002, 0.005, 0.010, 0.020) samples. The crystal structure of LiMn$_2$O$_4$ is shown in the inset. The enlargement of lattice parameters indicates that Bi and La enter into the spinel structure.

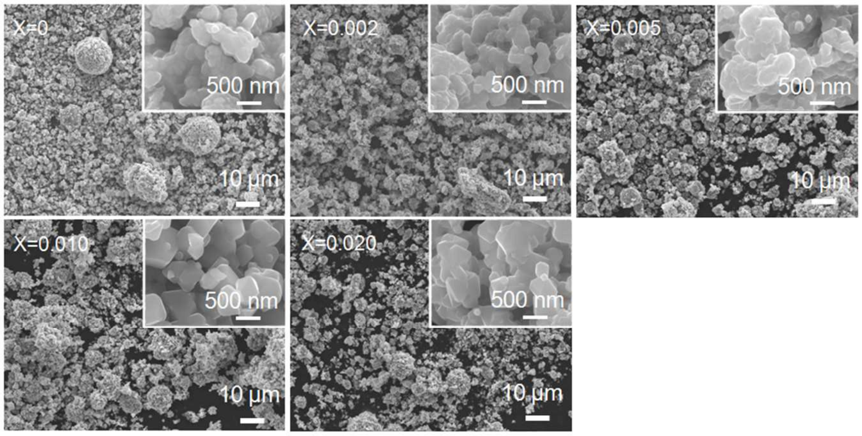

Fig. 3 SEM images of $LiBi_xLa_xMn_{2-2x}O_4$ (x=0, 0.002, 0.005, 0.010, 0.020) samples.

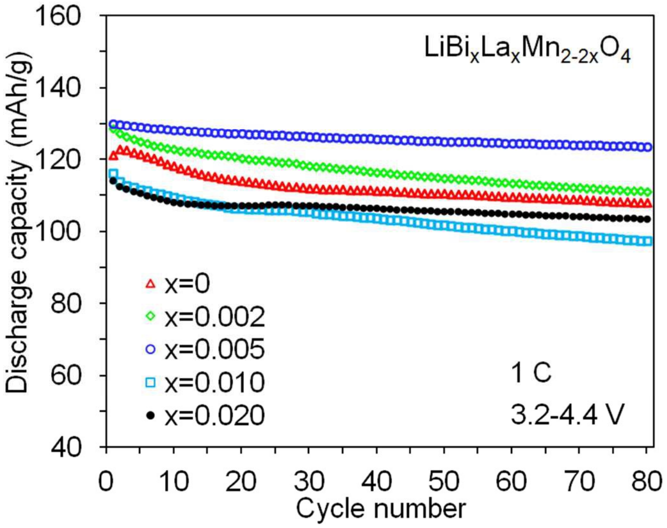

Fig. 4 Discharge capacity as a function of the cycle number for $LiBi_xLa_xMn_{2-2x}O_4$ (x=0, 0.002, 0.005, 0.010, 0.020) samples at 1 C between 3.2 and 4.4 V.

Table 1. Synthetic method and electrochemical properties of the current and reported works. SCS, S-G, and SSR represent the solution combustion synthesis, sol-gel, and solid state reaction, respectively.

Materials	Synthetic method	Current density	Voltage (V)	Discharge capacity(mAh/g)	Capacity retention	Ref.
$LiMn_2O_4$	SCS	1 C	3.2-4.4	116.3 (80 cycles)	89.0%	This work
$LiBi_{0.005}La_{0.005}Mn_{1.99}O_4$	SCS	1 C	3.2-4.4	123.7 (80 cycles)	95.0%	This work
$LiLa_{0.05}Mn_{1.95}O_4$	S-G	1 C	2.75-4.5	106 (50 cycles)	89.1%	26
$LiLa_{0.05}Mn_{1.95}O_4$	SSR	0.2 C	3.0-4.3	103.7 (100 cycles)	91.6%	27
Bi-modified $LiMn_2O_4$	S-G	~0.3 C	3.5-4.5	100 (100 cycles)	84.7%	37

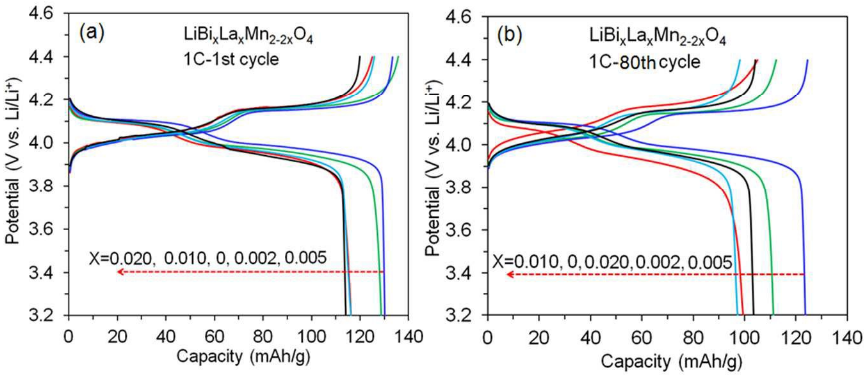

Fig. 5 Charge–discharge curves of $LiBi_xLa_xMn_{2-2x}O_4$ (x=0, 0.002, 0.005, 0.010, 0.020) samples at 1 C between 3.2 and 4.4 V. (a) the 1st cycle; (b) the 80th cycle.

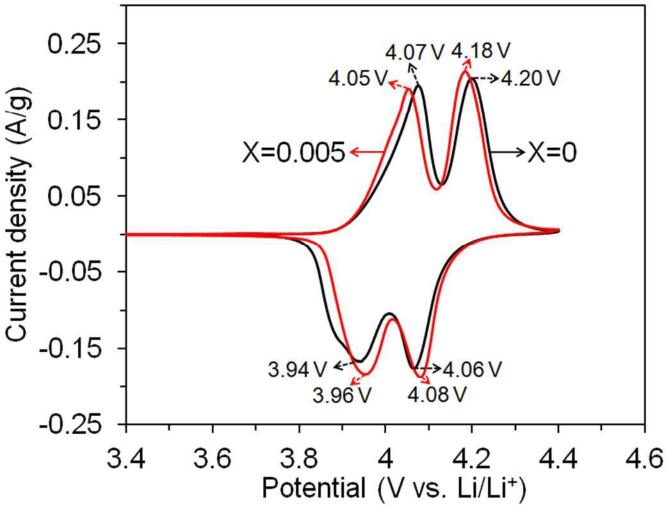

Fig. 6 Cyclic voltammetry (CV) curves of $LiBi_xLa_xMn_{2-2x}O_4$ (x=0, 0.005) samples in the voltage range of 3.2–4.4 V at a scan rate of 0.1 mV/s.

Table 2. Peak parameters of CV curves at the 1st cycle for the pristine $LiMn_2O_4$ and $LiBi_{0.005}La_{0.005}Mn_{1.99}O_4$ samples. ΔE_p is the separation between the anodic peak potential, $E_{pa,}$ and the cathodic peak potential, E_{pc}.

	Potential value (V)					
	E_{pa1}	E_{pa2}	E_{pc1}	E_{pc2}	ΔE_{p1}	ΔE_{p2}
x=0	4.07	4.20	3.94	4.06	0.13	0.14
x=0.005	4.05	4.18	3.96	4.08	0.09	0.10

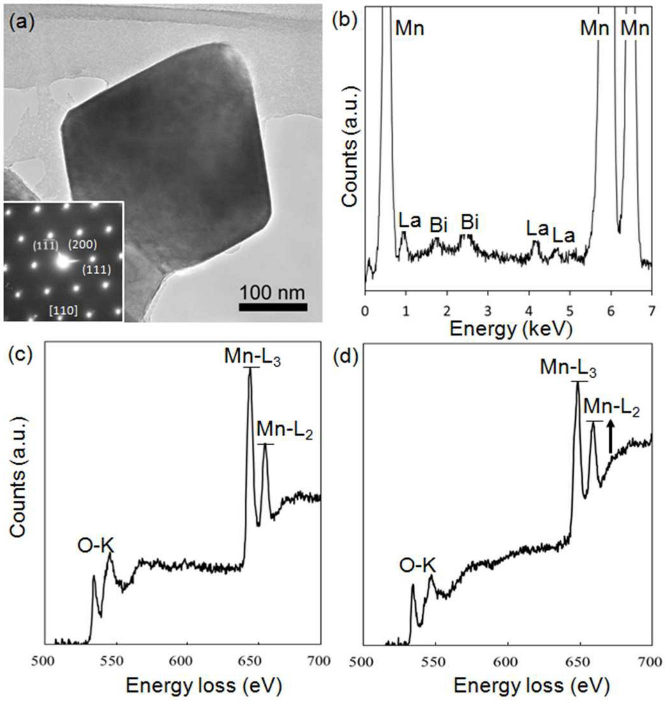

Fig. 7 The TEM image and electron diffraction pattern in [110] zone axis (a), and EDX analysis (b) of $LiBi_{0.005}La_{0.005}Mn_{1.99}O_4$ sample, in addition to the comparison of EEL spectra for $LiBi_xLa_xMn_{2-2x}O_4$ with $x = 0$ (c), and $x = 0.005$ (d).

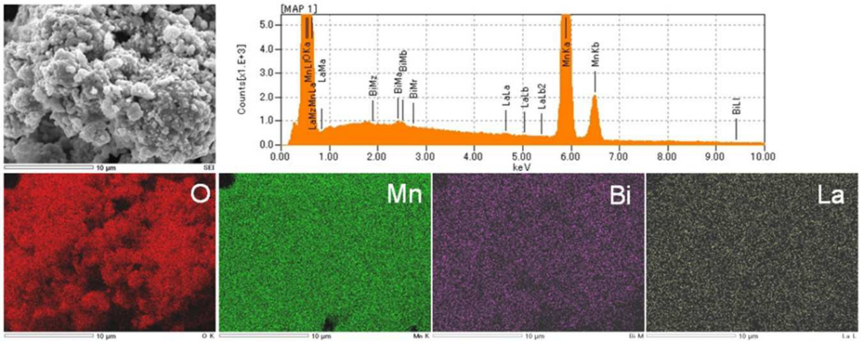

Fig. 8 EDS analysis of $LiBi_{0.005}La_{0.005}Mn_{1.99}O_4$ sample.

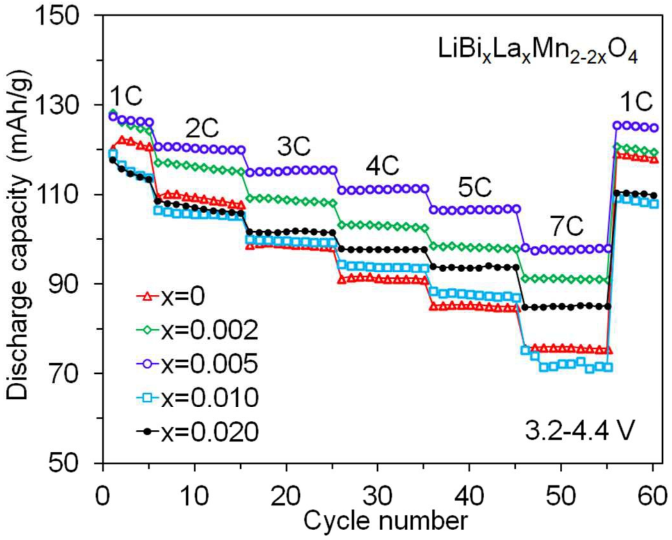

Fig. 9 Rate capability of LiBi$_x$La$_x$Mn$_{2-2x}$O$_4$ (x=0, 0.002, 0.005, 0.010, 0.020) samples.

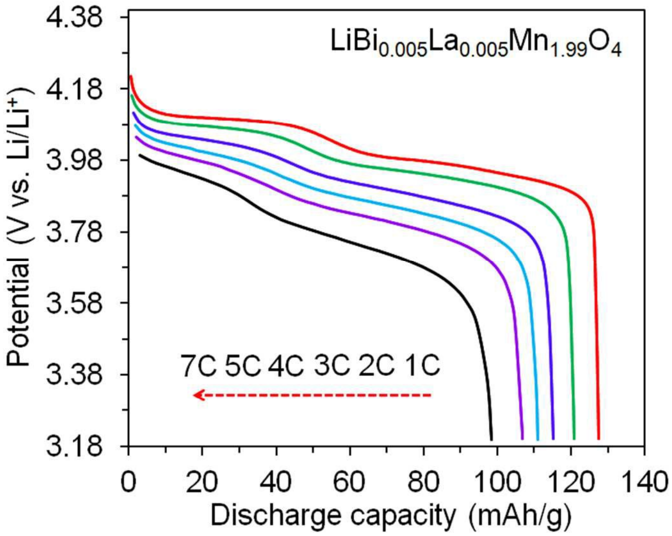

Fig. 10 Discharge curves at various current rates for LiBi$_{0.005}$La$_{0.005}$Mn$_{1.99}$O$_4$ sample.

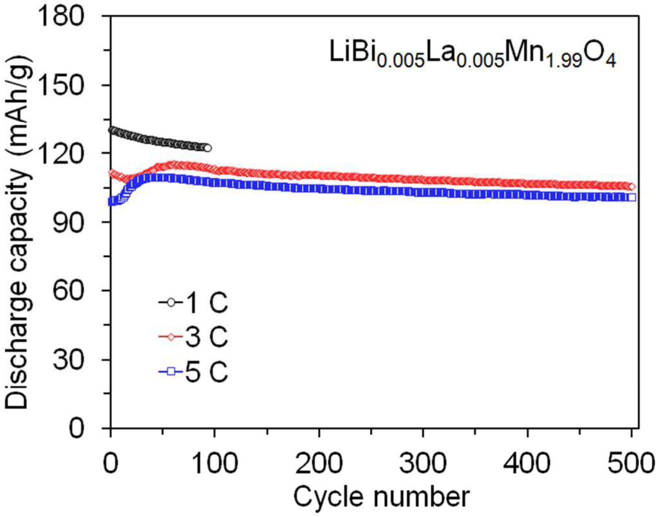

Fig. 11 Discharge capacity as a function of the cycle number for $LiBi_{0.005}La_{0.005}Mn_{1.99}O_4$ sample at 1 C, 3 C, and 5 C between 3.2 and 4.4 V.

Reference

1 M. Armand, J.M. Tarascon, *Nature*, 2008, **451**, 652–657.

2 P.G. Bruce, B. Scrosati, J.M. Tarascon, *Angew. Chem. Int. Ed.*, 2008, **47**, 2930–2946.

3 J.B. Goodenough, Y. Kim, *Chem. Mater.*, 2010, **22**, 587–603.

4 C.M. Hayner, X. Zhao, H.H. Kung, *Annu. Rev. Chem. Biomol. Eng.*, 2012, **3**, 445–471.

5 Y.L. Ding, J. Xie, G.S. Cao, T.J. Zhu, H.M. Yu, X.B. Zhao, *J. Phys. Chem. C*, 2011, **115**, 9821–9825.

6 A. Manthiram, A. Vadivel Murugan, A. Sarkar, T. Muraliganth, *Energy Environ. Sci.*, 2008, **1**, 621–638.

7 H.R. Lee, B. Lee, K.Y. Chung, B.W. Cho, K.-Y. Lee, S.H. Oh, *Electrochim. Acta*, 2014, **136**, 396–403.

8 R. Thirunakaran, R. Ravikumar, S. Vanitha, S. Gopukumar, A. Sivashanmugam, *Electrochim. Acta*, 2011, **58**, 348–358.

9 R.J. Gummow, A. Dekock, M.M. Thackeray, *Solid State Ionics*, 1994, **69**, 59–67.

10 Y.Y. Xia, Y.H. Zhou, M. Yoshio, *J. Electrochem. Soc.*, 1997, **144**, 2593–2600.

11 T. Qiu, J. Wang, Y. Lu, W. Yang, *Electrochim. Acta*, 2014, **147**, 626–635.

12 S. Hu, Y. Li, F. Lai, X. Zhang, Q. Li, Y. Huang, X. Yuan, J. Chen, H. Wang, *RSC Adv.*, 2015, **5**, 17592–17600.

13 Y. Xu, G. Chen, E. Fu, M. Zhou, M. Dunwell, L. Fei, S. Deng, P. Andersen, Y. Wang, Q. Jia, H. Luo, *RSC Adv.*, 2013, **3**, 18441–18445.

14 H. Zhao, X. Liu, C. Cheng, Q. Li, Z. Zhang, Y. Wu, B. Chen, W. Xiong, *J. Power Sources*, 2015, **282**, 118–128.

15 W. Wen, B. Ju, X. Wang, C. Wu, H. Shu, X. Yang, *Electrochim. Acta*, 2014, **147**, 271–278.

16 R. Singhal, S.R. Das, M.S. Tomar, O. Ovideo, S. Nieto, R.E. Melgarejo, R.S. Katiyar, *J. Power Sources*, 2007, **164**, 857–861.

17 P. Arora, B.N. Popov, R.E. White, *J. Electrochem. Soc.*, 1998, **145**, 807–815.

18 F.P. Nkosi, C.J. Jafta, M. Kebede, L. le Roux, M.K. Mathe, K.I. Ozoemena, *RSC Adv.*, 2015, **5**, 32256–32262.

19 A.B. Yuan, L. Tian, W.M. Xu, Y.Q. Wang, *J. Power Sources*, 2010, **195**, 5032–5038.

20 Y. Shi, S. Zhu, C. Zhu, Y. Li, Z. Chen, D. Zhang, *Electrochim. Acta*, 2015, **154**, 17–23.

21 N. Jayaprakash, N. Kalaiselvi, Gangulibabu, D. Bhuvaneswari, *J. Solid State Electrochem.*, 2011, **15**, 1243–1251.

22 A. Iturrondobeitia, A. Goñi, V. Palomares, I. Gil de Muro, L. Lezama, T. Rojo, *J. Power Sources*, 2012, **216**, 482–488.

23 D.-Q. Liu, Z.-Z. He, X.-Q. Liu, *J. Alloys Compd.*, 2007, **440**, 69–73.

24 M. Mo, K.S. Hui, X. Hong, J. Guo, C. Ye, A. Li, N. Hu, Z. Huang, J. Jiang, J. Liang, H. Chen, *Appl. Surf. Sci.*, 2014, **290**, 412–418.

25 S.R.K. Balaji, D. Mutharasu, S. Shanmugan, N.S. Subramanian, K. Ramanathan, *Ionics*, 2010, 16, 351–360.

26 D. Arumugam, G.P. Kalaignan, P. Manisankar, *Solid State Ionics*, 2008, **179**, 580–586.

27 H. Sun, Y. Chen, C. Xu, D. Zhu, L. Huang, *J. Solid State Electrochem.*, 2012, **16**, 1247–1254.

28 R.M. Rojas, J.M. Amarilla, L. Pascual, J.M. Rojo, D. Kovacheva, K. Petrov, *J. Power Sources*, 2006, **160**, 529–535.

29 F. Bonino, S. Panero, D. Satolli, B. Scrosati, *J. Power Sources*, 2001, **97–98**, 389–392.

30 R. Alcantara, M. Jaraba, P. Lavela, J.M. Lloris, C.P. Vicente, J.L. Tirado, *J. Electrochem. Soc.*, 2005, **152**, A13–A18.

31 H. Goktepe, H. Sahan, S. Patat, A. Ulgen, *Ionics*, 2009, **15**,233–239.

32 P. Mohan, B. Ranjith, G.P. Kalaignan, *J. Solid State Electrochem.*, 2014, **18**, 2183–2192.

33 A. Iqbal, Y. Iqbal, L. Chang, S. Ahmed, Z.Y. Tang, Y. Gao, *J. Nanopart. Res.*, (2012), **14**, 1-14 .

34 H.W. Liu, L. Song, K.L. Zhang, Er-doped LiMn2O4. *Inorganic Materials*, 2005, **41**, 646–649.

35 G.P. Nayaka, J. Manjanna, K.C. Anjaneya, P. Manikandan, P. Periasamy, V.S. Tripathi, Bull. Mater. Sci., 2014, **37**, 705–711.

36 H. Schlörb, M. Bungs, W. Plieth, *Electrochim. Acta*, 1997, **42**, 2619–2625.

37 C.L. Tan, H.J. Zhou, W.S. Li, X.H. Hou, D.S. Lue, M.Q. Xu, Q.M. Huang, *J. Power Sources*, 2008, **184**, 408–413.

38 H. Ahmad, N. Mohammad, Z. Sirus, *World Appl. Sci. J.*, 2012, **19**, 424–430.

39 H.L. Wang, T.A. Tan, P. Yang, M.O. Lai, L. Lui, *J. Phys. Chem. C*, 2011, **115**, 6102–6110.

40 C.-G. Han, C. Zhu, G. Saito, T. Akiyama, *Adv. Powder Technol.*, 2015, **26**, 665–671.

41 C. Zhu, A. Nobuta, G. Saito, I. Nakatsugawa, T. Akiyama, *Adv. Powder Technol.*, 2014, **25**, 342–347.

42 J.M. Tarascon, W.R. McKinnon, F. Coowar, T.N. Bowmer, G. Amatucci, D. Guyomard, *J. Electrochem. Soc.*, 1994, **141**, 1421–1431.

43 J.L. Wang, Z.H. Li, J. Yang, J.J. Tang, J.J. Yu, W.B. Nie, G.T. Lei, Q.Z. Xiao, *Electrochim. Acta*, 2012, **75**, 115–122.

44 K.J. Carroll, D. Qian, C. Fell, S. Calvin, G.M. Veith, M. Chi, L. Baggetto, Y.S. Meng, *Phys. Chem. Chem. Phys.*, 2013, **15**, 11128–11138.

45 R.D. Leapman, L.A. Grunes, P.L. Fejes, *Phys. Rev. B*, 1982, **26**, 614–635.

46 H.K. Schmid, W. Mader, *Micron*, 2006, **37**, 426–432.

47 T. Riedl, T. Gemming, K. Wetzig, *Ultramicroscopy*, 2006, **106**, 284–291.

48 H. Zhao, F. Li, X. Liu, C. Cheng, Z. Zhang, Y. Wu, W. Xiong, B. Chen, *Electrochim. Acta*, 2015, **151**, 263–269.